Applied Catalysis B: Environmental 138–139 (2013) 199–211

Contents lists available at SciVerse ScienceDirect

Applied Catalysis B: Environmental

journal homepage: www.elsevier.com/locate/apcatb

# Sulfation of $Pt/Al_2O_3$ catalyst for soot oxidation: High utilization of $NO_2$ and oxidation of surface oxygenated complexes

Shuang Liu [a], Xiaodong Wu [a,*], Duan Weng [a], Min Li [a], Jun Fan [b]

[a] The Key Laboratory of Advanced Materials of Ministry of Education, School of Materials Science and Engineering,Tsinghua University, Beijing 100084, China
[b] The Administrative Centre for China's Agenda 21, Beijing 100038, China

ARTICLE INFO

*Article history:*
Received 10 December 2012
Received in revised form 1 February 2013
Accepted 28 February 2013
Available online 6 March 2013

*Keywords:*
$Pt/Al_2O_3$
Sulfates
Diesel soot oxidation
Surface oxygenated complexes
$NO_x$ preferential adsorption

ABSTRACT

The sulfated $Pt/Al_2O_3$ catalyst was synthesized by impregnating $H_2SO_4$ on the $Pt/Al_2O_3$ catalyst. It exhibits higher catalytic activity than $Pt/Al_2O_3$ for soot oxidation under loose contact conditions in a feed flow containing NO and $O_2$. Further studies ascribe its good activity to a synergistic effect between sulfate species and platinum. Firstly, the electronegative sulfate species may improve the oxidation-resistance of metallic platinum in the oxidizing atmosphere, which is important for achieving high $NO \leftrightarrow NO_2 \leftrightarrow$ soot recycling efficiency; Secondly, the sulfate species inhibit the $NO_x$ adsorption on the alumina support, leading to a preferential adsorption of $NO_x$ on the surface of soot rather than on the catalyst, and thus provide more chances for $NO_2$-soot reaction to generate the surface oxygenated complexes (SOCs); Finally, the sulfate species can promote the further decomposition of these SOCs species, resulting in a high catalytic efficiency for soot oxidation.



## 1. Introduction

The different legislations dedicated to diesel particulate matter (PM) emissions of vehicles (for Europe, 0.005 g of particulates/km for passenger cars since 2009) have led to the development of different after-treatment technologies. PM is mainly constituted by carbonaceous particles (often called soot), originated from the incomplete in-cylinder oxidation of the fuel, with diameters ranging from few nanometers (10–20 nm) to up to hundreds of nanometers [1,2]. Diesel particulate filters (DPFs) are the most common devices for the collection of particulate matter for on-board diesel exhaust after-treatment. However, they eventually become blocked as the soot accumulates on the filter. The most plausible method for regenerating the filter is to use a catalyst that promotes soot oxidation at exhaust gas temperatures under engine operating conditions [3,4]. Under practical conditions occurring in a catalytic DPF, good contact conditions are very difficult to be reached due to the different orders of magnitude of the soot particle and the catalyst cluster sizes, which clearly hinder the overall activity of the catalyst. It has been observed that for the catalysts without high mobility, a loose-contact mode obtained by mixing soot and catalyst with spatula is comparable with the practical contact mode [5]. In this condition, the most of the carbon atoms are in contact with gaseous phase and, consequently, the soot oxidation temperature can be significant reduced due to the $NO_2$ produced over the catalyst [6,7]. Among the catalysts investigated, Pt exhibits a high level of catalytic activity by oxidizing NO in the exhaust gas to $NO_2$ [3,4], and Pt catalysts typically consist of Pt nanoparticles dispersed on a porous alumina support.

The presence of sulfur-containing compounds in fuel and lubricants has been reported to favor the formation of thermally stable sulfate species on the catalyst supports, and sulfur may also affect the metal functionality for NO and soot oxidation [3,8]. It has been reported that Pt catalysts supported on non-basic metal oxides ($Ta_2O_5$, $Nb_2O_5$, $WO_3$, $SnO_2$ and $SiO_2$) show high activities toward the oxidation of soot in the presence of $SO_2$, which is attributed to their non-basicity and negligible affinity toward $SO_3$ (or $H_2SO_4$), resulting in less poisoning of the supported Pt [3,5]. Then the influence of sulfur will be especially significant for the catalysts with supports that have high affinity for sulfur, such as $Al_2O_3$ [8].

Since $NO_2$ is determinant for initiating and continuing soot oxidation in the loose-contact mode, many efforts were focused on obtaining active catalysts for $NO_2$ production [9,10]. It has only been recently reported that the catalytic activity for NO oxidation did not exactly match the soot oxidation capacity of some $CeO_2$-based catalysts [11,12]. In our recent study, it was also observed that on the sulfated $Pt/Al_2O_3$ catalyst, the $NO_2$-assisted mechanism was no longer the sole variable for the catalytic oxidation of soot. It is suggested that a synergistic effect between platinum and sulfates on the sulfated $Pt/Al_2O_3$ catalyst may accelerate some rate-limiting steps, and the specific mechanism remains to be investigated [13].

* Corresponding author. Tel.: +86 10 62792375; fax: +86 10 62792375.
*E-mail address:* wuxiaodong@tsinghua.edu.cn (X. Wu).

0926-3373/$ – see front matter © 2013 Elsevier B.V. All rights reserved.
http://dx.doi.org/10.1016/j.apcatb.2013.02.053

Therefore, a systematic study is required about what kind of factors, whether it is surface/textural properties or different reaction pathways on the sulfated $Pt/Al_2O_3$ catalyst that influence the catalytic oxidation of soot in the presence of $NO_x$. For this purpose, three different samples were prepared as $Pt/Al_2O_3$, sulfated $Pt/Al_2O_3$ and sulfated $Al_2O_3$. The catalysts were characterized by a series of structural and surface property measurements, and further insight into the catalyzed soot oxidation mechanism was gained based on some in situ experimental results.

## 2. Experimental

### 2.1. Materials

The $Pt/Al_2O_3$ (PtAl) catalyst was prepared by impregnating $Pt(NO_3)_2$ (27.82 wt.%, Heraeus) on $\gamma$-$Al_2O_3$ powders (BASF, 150 $m^2$/g). The nominal loading amount of Pt was 1 wt.%. The impregnated powders were submitted to drying at 110 °C overnight and calcination at 500 °C for 2 h. The $H_2SO_4$-modified catalyst (SPtAl) was prepared by impregnating $H_2SO_4$ (98%, Beijing Modern Eastern) on the Pt supported alumina catalyst with a nominal weight ratio of $H_2SO_4$:$Al_2O_3$ = 1:19. Both catalysts were calcined at 500 °C for 2 h. As a reference, a 5 wt.% $H_2SO_4$-modified alumina (SAl) was prepared.

Printex-U (Degussa) was used as a model soot. Its particle size was 25 nm and the specific surface area was 100 $m^2$/g. For further comparison, soot containing various surface oxygen complexes (Nsoot) was obtained by treating the Printex-U in a 500 ppm $NO_2$/10% $O_2$/$N_2$ flow (200 ml/min) at 350 °C for 4 h.

### 2.2. Catalyst characterization

The powder X-ray diffraction (XRD) patterns were determined by a Japan Science D/max-RB diffractometer employing Cu-Ka radiation ($\lambda$ = 0.15418 nm). The X-ray tube was operated at 40 kV and 30 mA. The X-ray diffractograms were recorded at 0.02° intervals in the range of $20^\circ \leq 2\theta \leq 80^\circ$ with a scanning velocity of 4°/min.

The specific surface areas of the samples were measured using the $N_2$ adsorption isotherm at −196 °C by the four-point Brunauer–Emmett–Teller (BET) method using an automatic surface analyzer (F-Sorb 3400, Gold APP Instrument). The samples were degassed at 200 °C for 2 h prior to the measurements.

CO titration experiments were conducted in a fixed bed quartz reactor via a method as described in ref. [8]. The catalysts were subjected to an oxygen exposure at room temperature with 30% $O_2$/$N_2$ (300 ml/min) for 1 h. The flow was then switched to $N_2$ (300 ml/min) in order to purge out any residual gases from the oxygen pre-treatment, and the reactor temperature was set to 150 °C. At this titration temperature, the flow was changed to 1% CO/$N_2$ (100 ml/min), and the outlet $CO_2$ concentration was analyzed by an infrared spectrometer (MKS 2300). The $CO_2$ trace was followed until it decreased to below the detection limit. The resulting $CO_2$ trace was integrated and, assuming a reaction stoichiometry $CO + O\text{-}Pt_S \rightarrow CO_2 + Pt_S$, the total amount of oxygen on the Pt was calculated. At 150 °C, CO can titrate the oxygen monolayer completely from Pt, and hence, the $CO_2$ amount formed (or the atomic oxygen removed) will be the same as the number of exposed surface Pt atoms. It is thus possible to calculate the number of surface Pt atoms from the CO titration at 150 °C and consequently the Pt dispersion (ratio of surface Pt to total Pt). Mean Pt particle size ($D_{Pt}$) was determined from Pt dispersion data by assuming all surface Pt particles were spherical in shape.

Transmission electron microscope (TEM) images were taken using a FEI Tecnai $G^2$ 20 with an acceleration voltage of 200 kV. The size distribution of the platinum crystallites was determined by measuring 200 particles for each sample, and the mean Pt particle size was also calculated from these data.

Infrared (IR) spectra of CO adsorbed on the samples were recorded on a Nicolet 6700 FTIR spectrometer equipped with a MCT detector. After pretreatment in $N_2$ (50 ml/min) at 500 °C for 30 min, the sample was then cooled down to RT. The spectra were taken after exposing the catalyst to 1% CO/$N_2$ (50 ml/min) for 30 min followed by purging with $N_2$.

The diffuse reflectance infrared Fourier transformed spectra (DRIFTS) were recorded on the same apparatus. All the samples were diluted with inert $CaF_2$ to obtain a feasible signal-to-noise ratio, and were prepared with a weight ratio of soot:catalyst:$CaF_2$ = 1:10:100 (Even if the sample contains only soot or catalyst, it would still be diluted with $CaF_2$ at the same weight ratio). After pretreatment in $N_2$ (50 ml/min) at 500 °C for 30 min, the sample was then cooled down to RT. Then the spectra were recorded from 100 °C to 550 °C at an interval of 50 °C in different atmospheres. The heating rate was 10 °C/min.

Thermogravimetric (TG) analysis experiments were conducted on a METTLER Toledo thermogravimetric analyzer. For each experiment, 15 mg of the sample was heated from ambient to 1000 °C at a heating rate of 10 °C/min. Reaction was carried out in $N_2$ (50 ml/min) at the gauge pressure of 0.1 atm (10.1 kPa). The chamber blowing gas, $N_2$ (99.99% purity), was fixed at a flow rate of 20 ml/min.

The NO temperature-programmed oxidation (TPO) tests were carried out in a fixed-bed reactor with the effluent gases monitored by an infrared spectrometer (Thermo Nicolet IS10). 100 mg of sample was diluted with 300 mg of silica pellets, and then were sandwiched by quartz wool in a tubular quartz reactor. A gas mixture of 1000 ppm NO/10% $O_2$/$N_2$ (500 ml/min) was fed and the reactor temperature was ramped to 600 °C at a heating rate of 10 °C/min.

The $NO_x$ temperature-programmed desorption (TPD) tests were performed in the same apparatus to that used in NO-TPO tests. Prior to the test, the sample powders were exposed in 500 ppm $NO_2$/10% $O_2$/$N_2$ (500 ml/min) at 350 °C for 30 min then cooled down to RT in the same atmosphere and flushed by $N_2$. Afterwards, the NO and $NO_2$ desorption profiles were obtained by ramping the reactor from RT to 600 °C at a heating rate of 10 °C/min in a 10% $O_2$/$N_2$ stream.

### 2.3. Activity measurement

In the activity measurement, 10 mg of soot and 100 mg of sample were mixed by a spatula for 2 min for "loose contact" conditions. In order to prevent reaction runaway, 110 mg of the soot–catalyst mixture was diluted with 300 mg of silica pellets. The inlet gas mixture was either 1000 ppm NO/10% $O_2$/$N_2$ or 10% $O_2$/$N_2$ with a total flow rate of 500 ml/min, and the gas hourly space velocity (GHSV) was 30,000 $h^{-1}$. The activities of the catalysts for soot oxidation were evaluated in the same apparatus to that used in NO-TPO tests, and also in a temperature programmed oxidation (TPO) reaction apparatus at a heating rate of 10 °C/min. $T_{50}$ represented the temperature at which 50% of soot was oxidized. The downstream $CO_2/(CO_2 + CO)$ ratio during soot oxidation was defined as the selectivity to $CO_2$. The as-received catalysts were treated with soot under the same atmosphere from RT to 600 °C to obtain the spent catalysts with a suffix of "-s".

## 3. Results

### 3.1. Solid properties

Fig. 1 shows the XRD patterns of the catalysts. Only typical peaks of $\gamma$-$Al_2O_3$ are observed in the diffraction patterns of the catalysts

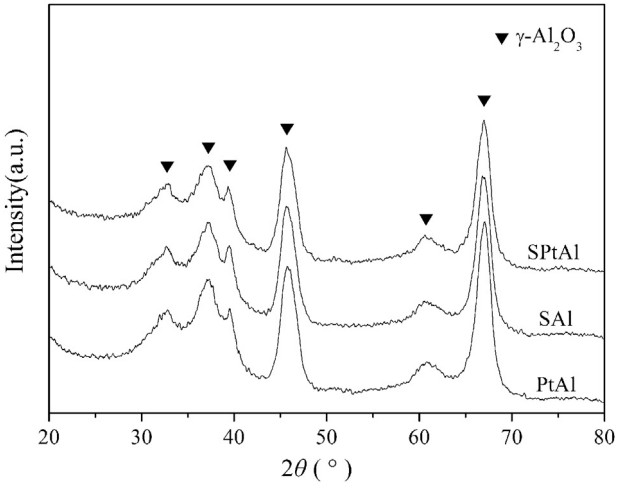


**Fig. 1.** XRD patterns of the catalysts.

and the sulfated support. Due to the influence of sulfate species, SPtAl and SAl show slightly lower crystallinity of γ-$Al_2O_3$ than PtAl. Similar phenomena have been discovered on the sulfated $TiO_2$, $ZrO_2$ and $SiO_2$ supports [14]. No characteristic peaks of sulfates or platinum species are found, indicating that these compounds are in high dispersion or low degree of crystallinity. As shown in Table 1, the surface sulfates introduced by impregnation of $H_2SO_4$ led to a slight decrease in the surface area of the catalyst, which comes from the blocking effect on the support pores. However, such slight variations in the catalyst surface area should not result in any obvious differences in the catalytic performance of the catalysts.

### 3.2. CO titration and TEM results

NO and soot catalytic oxidation over Pt catalysts is generally believed to depend strongly on the particle size of Pt [15,16]. As the Pt particles on PtAl and SPtAl are too small to be detected by XRD, CO titration was employed to measure the Pt dispersions. As shown in Table 1, the sulfation leads to a significant decrease in the amount of Pt surface area, which implies either the formation of large Pt particles or partial blocking of Pt sites by sulfates on the SPtAl catalyst.

To observe the actual Pt particle sizes on different catalysts and judge the specific factor accounting for the reduction of Pt surface area on the sulfated catalysts, high-resolution TEM images of the catalysts were obtained and shown in Fig. 2. The sizes of two hundred Pt dark particles were collected for each catalyst, the corresponding Pt particle size distribution (PSD) and the average platinum particle sizes are shown in Fig. 2 and Table 1, respectively. For the PtAl sample, the Pt particle size estimated by CO titration correlates well with that from TEM result. Meanwhile, a significant difference is attained between these two results for the SPtAl sample, indicating that the obvious decrease in Pt accessible

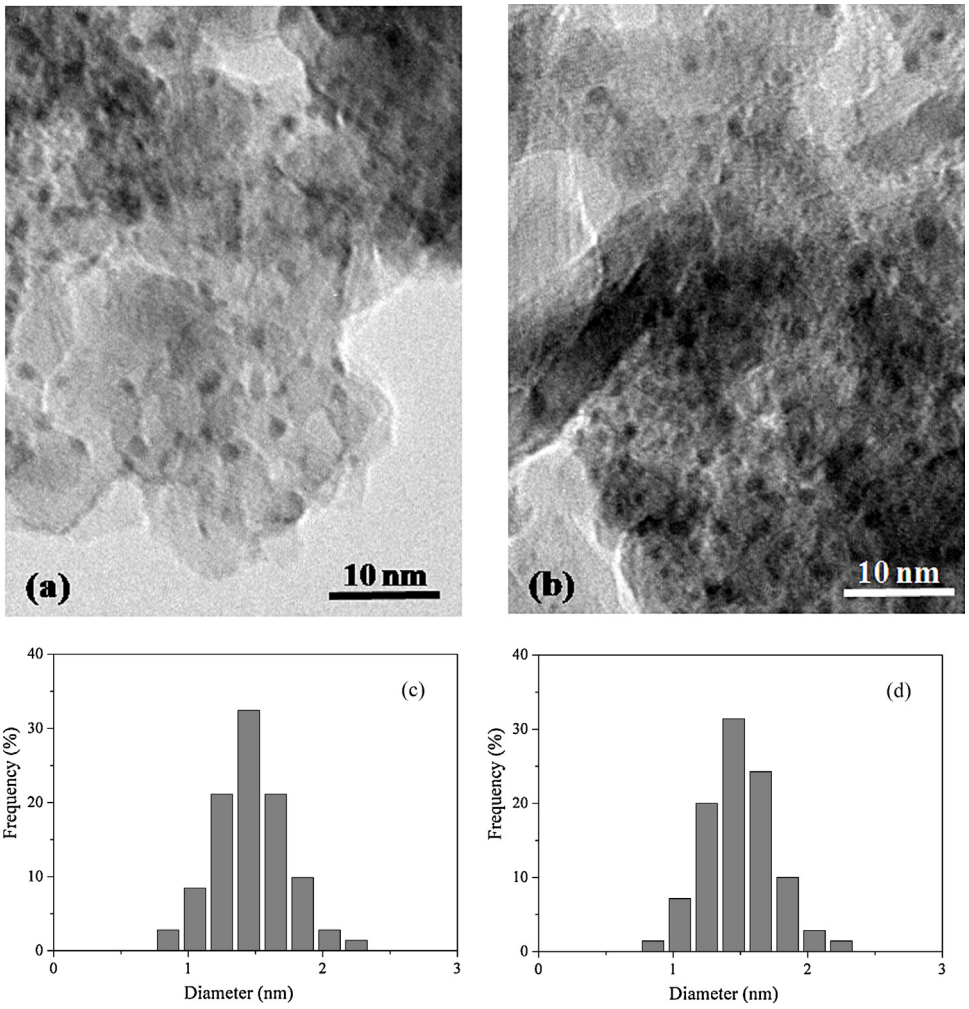


**Fig. 2.** TEM images and size distribution of Pt particles on (a), (c) PtAl and (b), (d) SPtAl.

**Table 1**
Overview of the structural properties of different samples.

| Catalyst | $S_{BET}$ ($m^2$/g) | Pt dispersion[a] (%) | $D_{Pt}$ from CO/Pt[a] (nm) | $D_{Pt}$ from TEM[b] (nm) |
|---|---|---|---|---|
| PtAl | 142 | 82 | 1.4 | 1.5 |
| SPtAl | 124 | 43 | 2.7 | 1.5 |
| SAl | 121 | – | – | – |

[a] Obtained from the CO titration results.
[b] Mean Pt particle size estimated from TEM results.

area measured by CO titration does not originate from the particle growth of Pt, but primarily from the surface coverage by sulfates. As PtAl and SPtAl exhibit similar Pt particle size distributions, the particle size effect of Pt is likely to be ruled out in this work.

### 3.3. IR spectra of CO adsorption

Besides the Pt particle size, the oxidation state of platinum may also be influenced by the introduction of sulfates. Fig. 3 shows the IR spectra of CO adsorbed on the catalysts at room temperature. The PtAl catalyst exhibits three overlapped bands at 2111, 2082 and 2063 $cm^{-1}$ which are assigned to CO linearly adsorbed on Pt electron-deficient clusters ($Pt^{\delta+}$), terrace and step sites of $Pt^0$ crystallites, respectively [17]. The band at 2111 $cm^{-1}$ shifts toward a higher wavenumber (2128 $cm^{-1}$) on the sulfated sample due to the more electron-deficient state of platinum on the acidic support [18]. Compared with the PtAl sample, SPtAl totally lost the $Pt^0$ band at 2063 $cm^{-1}$ due to the surface coverage of Pt by sulfate species. No obvious CO adsorption is detected on the SAl sample in the wavenumber range between 2000 and 2250 $cm^{-1}$.

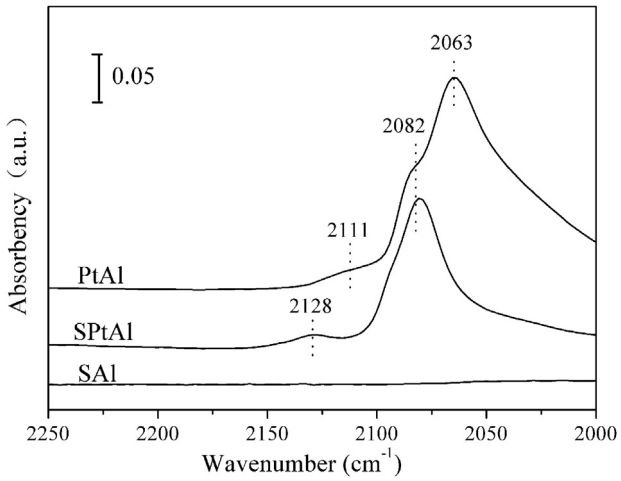


**Fig. 3.** IR spectra of CO adsorption on the different catalysts.

### 3.4. Ex situ IR spectra and thermal analysis

Infrared spectrum is an effective technique to detect the formation of sulfates. Fig. 4a shows the IR spectra of the as-received PtAl, SPtAl and SAl catalysts. For PtAl, the distinct band at 1044 $cm^{-1}$ is assigned to the OH-bending vibration of hydrated alumina surface [19,20], and this band shifts to 1013 $cm^{-1}$ on the sulfated samples probably due to the electron-withdrawing character of the sulfates. After sulfation, three overlapped adsorption bands at 1068, 1176 and 1283 $cm^{-1}$ are observed on SPtAl, which can be associated with a surface sulfate species or a sulfite species and a tri-coordinated sulfate species on alumina, respectively [21]. The band centered at 1283 $cm^{-1}$ on SPtAl is much weaker than that on the SAl sample, which should be due to the severe water absorbance in air on the surfaces of the platinum-containing sample and hereby the

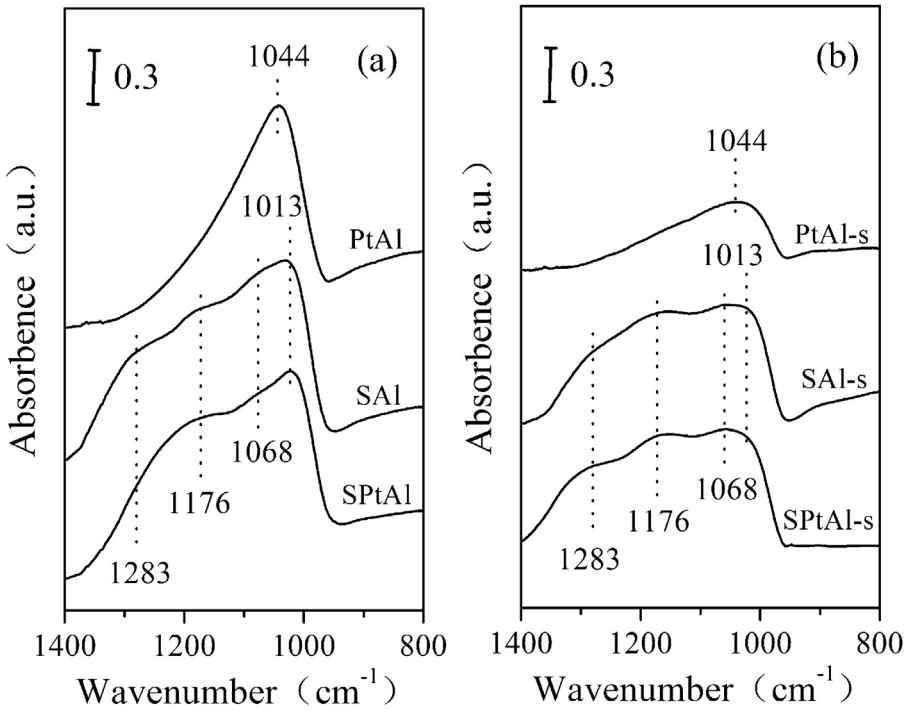


**Fig. 4.** IR spectra of the (a) as-received and (b) spent catalysts.

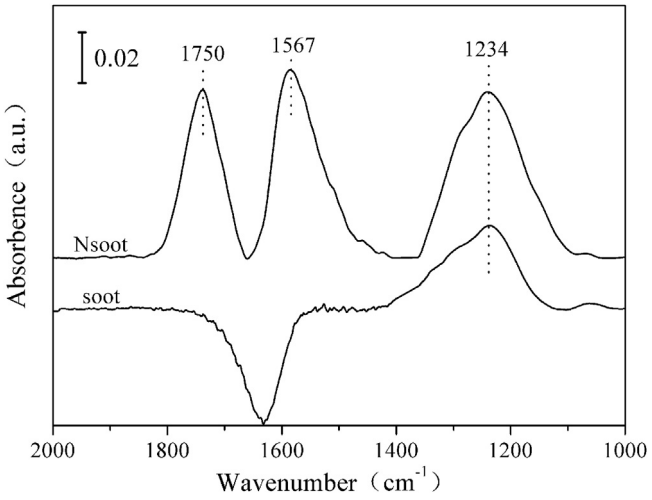


**Fig. 5.** IR spectra of the untreated Printex-U and Nsoot.

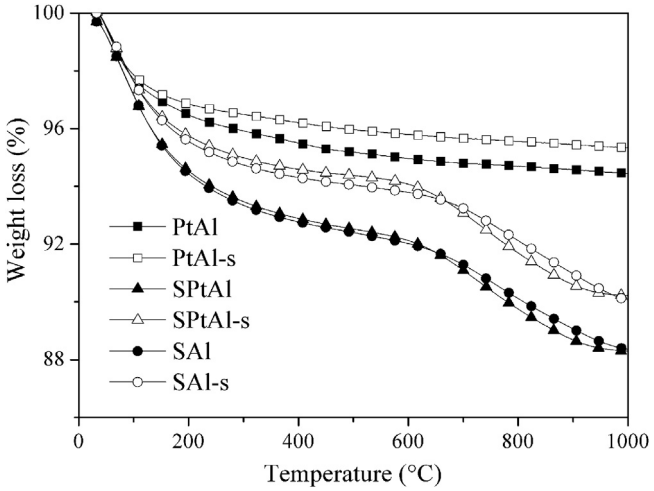


**Fig. 6.** TGA curves of the catalysts.

**Table 2**
IR assignments for surface oxygenated carbon complexes.

| Band positions ($cm^{-1}$) | Surface oxygen complexes | Modes | Reference |
|---|---|---|---|
| 1850–1776 | Anhydride | ν(C═O) | [23–26] |
| 1310–1210 | | ν(C—O) | |
| 1765–1745 | Lactone | ν(C═O) | [23–26] |
| 1370–1160 | | ν(C—O) | |
| 1720–1668 | Carboxylic | ν(C═O) | [23–25,27] |
| 1200–1120 | | ν(C—O) | |
| 1590 | Quinone | ν(C═C) | [23] |
| 1275–1200 | Ether | ν(C—O—C) | [23] |
| 1635 | Carbonyl | ν(C═O) | [23] |
| 1310 | Phenol | ν(O—H) | [23] |
| 1230 | | ν(C—O) | |

decrease in the intensity of the S—OH band [22]. After the soot-TPO reaction, the band (1044–1013 $cm^{-1}$) associated with OH-bending vibration decreases significantly in intensity on all the spent samples. The stronger band at 1283 $cm^{-1}$ on SPtAl-s than on SPtAl is attributed to the more serious dehydration during the reaction. All the bands assigned to sulfates maintain on the spent catalysts, indicating that the sulfate species on the surface of the catalysts would always exist during the soot catalytic oxidation reactions.

Fig. 5 shows the IR spectra of untreated Printex-U (denoted as "soot") and Nsoot. Typical wavenumbers of carbon–oxygen complexes are summarized in Table 2. It is shown that a very low intensity of carbon–oxygen complexes have already existed on untreated Printex-U with a band centered at around 1234 $cm^{-1}$. The $NO_2$-pretreated Nsoot shows three broad bands in the range of 1840–1659, 1650–1409 and 1359–1150 $cm^{-1}$ associating with surface carbon–oxygen complexes (anhydride, lactones and carboxylic species), with obvious higher intensities than those on the untreated Printex-U. It cannot be ruled out for the existence of surface nitrates since their absorption bands (at around 1600, 1300 and 1200 $cm^{-1}$) are overlapped with those of the surface oxygenated complexes. The IR results indicate that the pretreatment in $NO_2$ led to partially oxidation of Printex-U and the formation of surface oxygen complexes on the Nsoot [23–26].

In order to judge the degree of sulfation and possible desulfation of the catalysts during the catalytic reaction, the TGA curves of the sulfated catalyst before and after soot-TPO tests were measured and the results are shown in Fig. 6. The dehydration process is observed at the temperatures below 300 °C for all the samples. It can be seen that the weight loss due to dehydration is smaller on all the spent catalysts compared with the fresh sample, which is ascribed to the dehydration during the soot-TPO reaction. It is noted that SPtAl experienced more serious dehydration than SAl, which is in accord with the ex *situ* IR results. This extra dehydration may be ascribed to a participation of surface or bulk $H_2O$ located on the of SPtAl in the soot oxidation reaction, which is reported important for the deep oxidation of the SOCs [3,28]. The decomposition of sulfates in SPtAl and SAl starts at around 600 °C, the weight losses due to sulfate decomposition are about 3.9% for both SPtAl and SAl. By assuming the gaseous species formed in TGA to be $SO_2/SO_3$ and $O_2$, the actual loading amount of sulfates would be 4.7%, which is slightly smaller than the nominal content of $H_2SO_4$ (5%). After soot-TPO tests in $NO + O_2$, the weight loss due to sulfate decomposition are 3.8% and 3.6% for the SPtAl-s and SAl-s catalysts, respectively, which are similar to the value for the as-received catalyst and sulfated support. It indicates that little sulfate species had decomposed during the soot oxidation process, which agrees well with the ex *situ* IR results.

### 3.5. Catalytic activities for soot and NO oxidation

Figures S1–S4 show the TPO profiles of catalyzed and uncatalyzed soot oxidation in different conditions, and the data of light-off temperature $T_{50}$ are shown in Table 3. In the presence of NO, the catalytic activity of SPtAl is clearly higher than that of PtAl, indicating a significant promotion effect of sulfates on the soot oxidation activity of $Pt/Al_2O_3$ catalyst. All the platinum-containing catalysts yield a high $CO_2$ selectivity (>98%), while the SAl sample only exhibits $CO_2$ selectivity of ca. 90% under all the reaction conditions. It is noted that the SAl sample shows very low activity with the $T_{50}$ close to that of uncatalyzed reaction, which indicates the superior activity of SPtAl is most likely due to the synergistic effect of sulfates and platinum rather than any possible interaction between sulfates and alumina. In the absence of $NO_x$, the soot oxidation activity of the platinum-containing catalysts decreased dramatically, and the catalytic activity of $Pt/Al_2O_3$ is slightly weakened by the addition of sulfates, which should be due to the smaller exposed Pt surface area on the sulfated sample. That is, the high activity of the platinum-containing catalysts, especially the promoting effect of sulfates on the $Pt/Al_2O_3$ sample is closely related with the $NO_x$ utilization in the soot oxidation reactions.

Since $NO_2$ is determinant for initiating and continuing soot oxidation in the loose-contact mode, the oxidation of NO to $NO_2$ is an important step in soot catalytic oxidation in $NO + O_2$ [11,23]. Fig. 7a shows the evolution of the outlet $NO_2$ concentration during the NO-TPO measurements. The NO oxidation activity of SPtAl was deactivated by the surface coverage of sulfates (confirmed by the difference of Pt particle size values obtained by CO titration

**Table 3**
$T_{50}$ of the catalysts in soot-TPO in different atmospheres (°C).

| Catalyst | 1000 ppm NO/10% $O_2/N_2$ | | 10% $O_2/N_2$ | |
|---|---|---|---|---|
| | Catalyst + soot | Catalyst/soot[a] | Catalyst + soot | Catalyst + Nsoot |
| PtAl | 464 | 551 | 515 | 525 |
| SPtAl | 430 | 567 | 528 | 516 |
| SAl | 563 | – | 568 | 557 |
| Uncatalyzed | 570 | – | 575 | 572 |

[a] Obtained from the soot-TPO tests performed in "non-contact" mode.

and TEM results) and the partially oxidation of Pt (confirmed by CO-IR results) [29]. Fig. 7b shows the corresponding evolutions of $NO_2$ during the soot-TPO tests with different catalysts. Almost no $NO_2$ is observed in the outlet gas for both PtAl and SPtAl, indicating the total consumption of $NO_2$ by reaction with soot in the "non-contact" mode. For the soot-TPO reactions performed in a loose-contact mode, it can be seen by comparison with the NO-TPO profiles (Fig. 7a) that the $NO_2$ gap between these two tests over SPtAl is much smaller than that over PtAl. Despite its lower NO oxidation activity, SPtAl exhibits a higher activity for soot oxidation and a higher $NO_2$ slip in the soot-TPO reaction. This discrepancy may be due to the improvement by Pt-sulfates interaction which counteracts the negative influence of the weakened NO oxidation activity. To further confirm this speculation and explore the specific mechanisms for the higher soot oxidation activity of SPtAl, a series of in situ tests were performed.

It has been reported that in the catalytic oxidation of soot, the further oxidation of the intermediate products that formed on soot during the reaction might be an important step [23]. To evaluate the influence of the different catalysts on the deep oxidation of soot, and rule out the disturbance of $NO_x$, the $NO_2$-pretreated Nsoot was used in the soot-TPO tests in 10%$O_2/N_2$. As shown in Table 3, PtAl exhibits a worse catalytic activity for Nsoot oxidation with the $T_{50}$ shifting toward high temperature by ca. 10 °C in respect to the catalytic oxidation of the untreated soot. On the contrary, the pretreatment of soot in $NO_2$ decreases the light-off temperature of SPtAl and SAl, which indicates that an accelerating effect on the deep oxidation of soot occurred on both the sulfate-related interfacial active sites.

Although the TGA results indicate that hardly any sulfate species decomposed during the soot oxidation process, there are still some differences between the weight loss of the as-received and spent catalysts. To confirm the influence of possible gaseous sulfur oxides generated by the sulfates decomposition, the soot-TPO tests were performed in a "non-contact" mode, in which the catalysts was placed upstream of soot and quartz wool was used to separate the them. The soot bed contained 10 mg of soot and 300 mg of silica pellets, while the catalyst bed contained 100 mg of catalyst (PtAl or SPtAl). Then the soot conversion profiles were obtained by ramping the reactor from RT to 650 °C at a heating rate of 10 °C/min in a 1000 ppm NO/10% $O_2/N_2$ stream. As shown in Table 3, the soot oxidation activities of the platinum-containing catalysts are inhibited to a large extent in the "non-contact" soot-TPO reaction, and the advantage of sulfated sample disappears. The SPtAl sample with lower $NO_2$ generation ability exhibits a worse activity than the PtAl sample. Thus, a close contact between catalyst and soot, i.e. the surface interaction between sulfates and soot, becomes a key factor responsible for the high soot oxidation activity of the SPtAl sample.

### 3.6. Isothermal soot and NO oxidation reactions

The intrinsic activity of catalyst is based on turnover frequency (TOF), which is defined as the ratio of reaction rate to the active site density of catalysts. The reaction rate of soot oxidation was determined by an isothermal reaction at 300 °C, at which temperature the soot conversion is low (<5%) and nearly constant over time (Figs. S5 and S6), and the temperature increase of the diluted catalyst bed was not found. The reaction rate for soot oxidation (the concentration of $CO_2$ per unit time) was calculated according to the slope of the lines, and the dispersion values estimated by the CO titration were used to normalize the rates as indicated in ref. [8]. The obtained results are shown in Table 4.

It is seen that the platinum-containing catalysts can accelerate the soot oxidation effectively, either in the presence or absence of $NO_x$, while the SAl catalyst has almost no catalytic activity except for the Nsoot reaction. Again, the latter case confirms the promotion effect of sulfates on the decomposition of SOCs on the $NO_x$-pretreated soot. This effect of sulfates is also observed by the comparison between PtAl and SPtAl. At a low temperature as 300 °C, the reaction rates for soot oxidation over the PtAl catalyst are always higher than those of the SPtAl catalyst except in the reactions performed with Nsoot.

When the total numbers of exposed surface atoms of Pt nanoparticles is taken into account, the promotion effect of sulfates is more significant. The lower Pt dispersion in SPtAl results in higher TOF values for the oxidation of soot in the presence of NO and $O_2$ and especially that of Nsoot in the presence of $O_2$, which is in agreement with the soot-TPO results and verifies the advantage of the sulfated SPtAl catalyst in the decomposition of SOCs. On the other hand, the

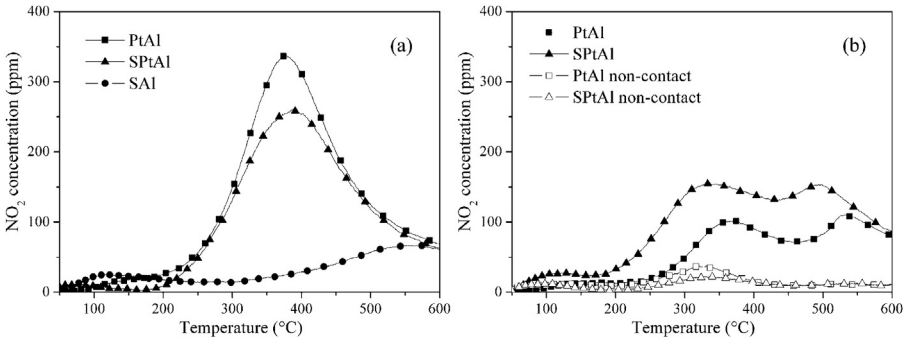


**Fig. 7.** $NO_2$ profiles during temperature-programmed oxidation of (a) NO and (b) soot. Reactant gas: 1000 ppm NO/10% $O_2/N_2$.

**Table 4**
The reaction rate and TOF values for soot oxidation over the PtAl and SPtAl catalysts at 300 °C.

| | Catalyst | 1000 ppm NO/10% $O_2/N_2$ | | 10% $O_2/N_2$ | |
|---|---|---|---|---|---|
| | | Catalyst + soot | Catalyst/soot[a] | Catalyst + soot | Catalyst + Nsoot |
| $R$ (mol/min × $10^{-6}$) | PtAl | 0.94 | 0.12 | 0.39 | 0.23 |
| | SPtAl | 0.70 | 0.06 | 0.2 | 0.48 |
| | SAl | 0.03 | – | 0.02 | 0.10 |
| | Uncatalyzed | 0.02 | – | 0.02 | 0.02 |
| $TOF_{Pt}$($s^{-1}$ × $10^{-3}$) | PtAl | 3.73 | 0.47 | 1.55 | 0.93 |
| | SPtAl | 5.29 | 0.44 | 1.48 | 3.63 |

[a] Obtained from the isothermal soot oxidation tests performed in "non-contact" mode.

TOF values of two catalysts are similar to each other both in loose contact condition in $O_2$ and in the "non-contact" mode in NO + $O_2$. This, again, highlights the importance of gaseous $NO_x$ species and the contact between catalysts and soot.

The TOF values for NO oxidation were obtained by the isothermal NO oxidation reaction at 375 °C, at which the NO oxidation rate was maximal for both PtAl and SPtAl as revealed in the NO-TPO profiles (Fig. 7). The reaction rate for NO oxidation (the concentration of $NO_2$ per unit time) was calculated according to the slope of the NO conversion lines (Fig. S7), and the Pt dispersion values estimated by the CO titration were used to normalize the rates. The reaction rate for NO oxidation is $0.78 \times 10^{-6}$ and $0.47 \times 10^{-6}$ mol/min for PtAl and SPtAl, respectively, indicating a lower activity of the sulfated catalyst for NO oxidation. The calculated TOF values are $3.2 \times 10^{-3}$ and $3.0 \times 10^{-3}$ $s^{-1}$ for PtAl and SPtAl, respectively. It agrees well with the results obtained by Pazmiño et al. [8] that the sulfur addition would not influence catalyst deactivation of Pt catalysts, resulting in unchanged turnover rates. They suggested that sulfur adsorbed preferentially on kinetically irrelevant sites, namely sites that become inactive even in the absence of sulfur, or sulfur may also adsorb on active sites but it is displaced by oxygen shortly after introducing the reactants such that the observed rates are effectively equal. Thus, the lower NO oxidation activity of SPtAl seems to come mainly from its lower Pt accessible surface area.

### 3.7. *In situ DRIFTS in 1000 ppm NO/10% $O_2/N_2$*

The addition of sulfates into $Pt/Al_2O_3$ catalysts may change the reaction routes of soot catalytic oxidation. To judge this point of view, in situ FTIR experiments were recorded for PtAl and SPtAl with or without soot in the presence of NO and $O_2$. The DRIFT spectra of adsorbed species on the soot-free catalyst and catalyst + soot mixtures arising in the reaction atmosphere (1000 ppm NO/10% $O_2/N_2$) were recorded and the results are shown in Fig. 8. Obtained results confirmed the formation of nitrites, nitrates and some surface oxygen complexes on the catalyst surface. A summary of the bands assignments used in this work is presented in Table 5.

In absence of soot, PtAl (Fig. 8a) mainly exhibits bands corresponding to chelating bidentate nitrates (1546 and 1329 $cm^{-1}$) and bridging bidentate nitrates (1619 and 1229 $cm^{-1}$) on alumina. All the bands increase in intensity with temperature ramping from 100 to 250 °C. Then at higher temperatures, with the decomposition of nitrates, the bands drop intensely in intensity and totally disappear at 500 °C. The band at ca. 1407 $cm^{-1}$ can be assigned to nitro compounds, which are unstable and quickly transformed to the nitrates species with ramping the temperature. Compared with nitrate bands on PtAl, due to the influence of sulfate species on the catalyst surface, those bands all exhibit a much lower intensity on SPtAl and experience a red shift (Fig. 8c), indicating that the surface sulfur complexes strongly inhibit the adsorption of $NO_x$ on the catalyst. The negative band at 1400–1385 $cm^{-1}$ comes from the alteration of the $SO_4^{2-}$ groups during $NO_x$ adsorption. The electronegative nitrate species affect the topmost $SO_4^{2-}$ groups through an induction effect, which causes a shift of the band due to the $\nu$(S=O) mode to lower frequency (the positive absorption bands at 1356 and 1204 $cm^{-1}$) [30].

As shown in Fig. 8b and d, due to the strong light-absorbance property of soot, the catalyst + soot mixtures exhibit much lower band intensity than the soot-free samples. After mixed with soot, three extra broad peaks at ca. 1365, 1580 and 1768 $cm^{-1}$ appear at temperatures higher than 300 °C. As illustrated in Fig. 8e, the soot sample exhibits only these three bands at high temperatures (though in lower intensity due to a stronger light-absorbance), so they can be associated with the surface oxygen complexes such as anhydride, lactones and/or carboxylic species that formed on the surface of soot, which are mainly formed as intermediate products of the partially oxidation of soot by $NO_x$ and $O_2$ [23,24]. However, these bands were not observed on the SPtAl + soot mixtures, indicating that the sulfate species either inhibited the formation of the SOCs, or accelerated the decomposition of these species. According to the results of the Nsoot-TPO tests, the latter case is more plausible.

### 3.8. *In situ DRIFTS in 1000 ppm $NO_2$/10% $O_2/N_2$*

To further discuss the influence of $NO_x$ species on soot catalytic oxidation, the DRIFT spectra were collected in a $NO_2$-rich atmosphere (1000 ppm $NO_2$/10% $O_2/N_2$). It is seen in Fig. 7 that the maximal $NO_2$ concentrations that generated in the NO-TPO over PtAl and SPtAl are no more than 400 ppm. It means that the concentration of 1000 ppm $NO_2$ is far beyond the possible amount of $NO_2$ that produced during the reaction, which may amplify the absorbance phenomenon and eliminate the discrepancy in NO oxidation activity of different catalysts.

As shown in Fig. 9a and c, compared with the spectra collected in NO + $O_2$ (Fig. 8), the sufficient $NO_2$ led to a stronger absorption intensity and some extra nitrate bands at ca. 1590, 1370 and 1312 $cm^{-1}$ on the soot-free PtAl and SPtAl catalysts. Similar phenomena appear on the catalyst + soot mixtures. Again, the bands at 1580 and 1768 $cm^{-1}$ assigned to surface oxygen complexes were also observed on the SPtAl + soot mixture (Fig. 9a). This indicates that sufficient $NO_2$ led to a fast formation of the SOCs species, and the promoting effect of sulfate species on the decomposition of these species could no longer catch their formation rate.

On the other hand, due to the stronger adsorption of $NO_x$ species, the difference of these species becomes more significant between on the sulfated and on the unsulfated samples. As shown in Fig. 9a and c, the chelating bidentate nitrates (1590, 1546 and 1329 $cm^{-1}$) seem to be the dominant nitrate species on PtAl, while the bridging bidentate nitrates (1626 and 1312 $cm^{-1}$) are the main nitrate species on SPtAl. When the soot was added, little change was observed on the $NO_x$ species of the PtAl sample. Meanwhile, the SPtAl sample exhibits much stronger adsorption bands at 1346 and 1204 $cm^{-1}$. These adsorption bands, corresponding to either surface nitrate or bridging bidentate nitrite as shown in Table 3, also exist in strong intensity on pure soot (Fig. 9e). That is, the

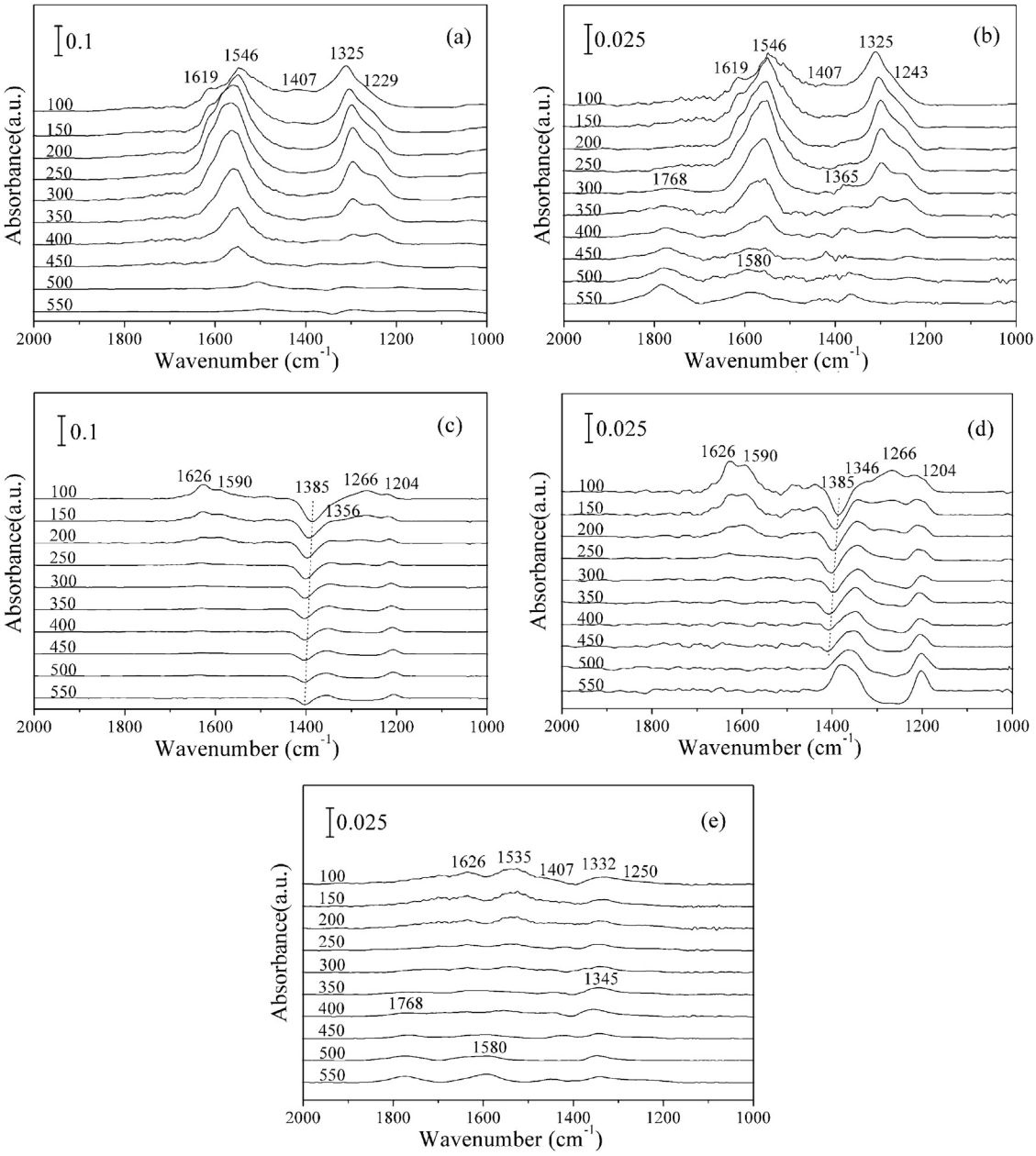


**Fig. 8.** DRIFT spectra recorded over (a) PtAl catalyst, (b) PtAl + soot mixture, (c) SPtAl catalyst, (d) SPtAl + soot mixture and (e) soot exposed to 1000 ppm NO/10% $O_2/N_2$ at different temperatures.

modification of sulfates for $Pt/Al_2O_3$ catalyst promotes the $NO_x$ adsorption from the catalyst to soot particles.

It has been stated that the $NO_2^+$ species is an important intermediate that facilitates the oxidation of soot [28]. As shown in Fig. 10a and c, the bands assigned to $NO_2^+$ at 2133 $cm^{-1}$ can be observed on both PtAl and SPtAl when exposed to 1000 ppm $NO_2$/10% $O_2/N_2$ [33]. The $NO_2^+$ band on PtAl decreases in intensity with increasing the temperature and disappears completely at 300 °C. For SPtAl catalyst, it maintains certain intensity even at 550 °C, with the band position shifting toward lower wavenumbers. These indicate the

**Table 5**
IR assignments for adsorbed $NO_x$ species.

| Band positions ($cm^{-1}$) | $NO_x$ species | Modes | Reference |
|---|---|---|---|
| 1640–1610 | Bridging bidentate nitrate | $\nu$(N=O) | [25,30–34] |
| 1270–1210 | | $\nu(NO_{2as})$ | |
| 1590–1540 | Chelating bidentate nitrate | $\nu$(N=O) | [25,26,31,32,34,35] |
| 1340–1280 | | $\nu(NO_{2as})$ | |
| 1325–1300 | Bridging bidentate nitrite | $\nu(NO_{2as})$ | [30–34] |
| 1230–1205 | | $\nu(NO_{2sym})$ | |
| 1550, 1257 | Monodentate nitrate | $\nu(NO_{2as})$, $\nu(NO_{2sym})$ | [31,34,36] |
| 1440–1325 | Nitro compound | $\nu(NO_{2as})$, $\nu(NO_{2sym})$ | [30,33] |

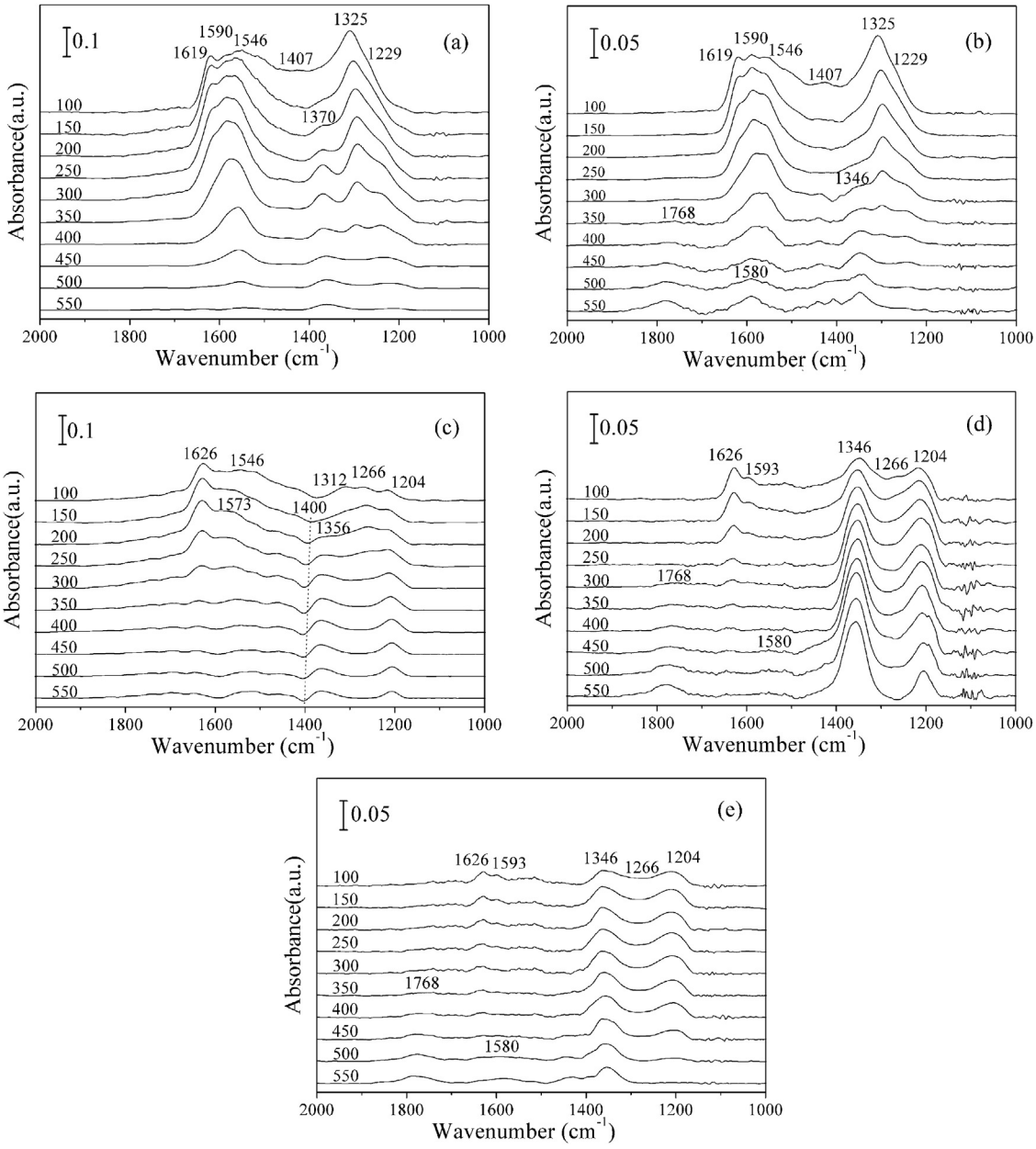


**Fig. 9.** DRIFT spectra between 2000 and 1000 $cm^{-1}$ recorded over (a) PtAl catalyst, (b) PtAl + soot mixture, (c) SPtAl catalyst, (d) SPtAl + soot mixture and (e) soot exposed to 1000 ppm $NO_2$/10% $O_2$/$N_2$ at different temperatures.

enhanced stability of $NO_2^+$ on the sulfated catalyst. Since the $NO_2^+$ species is highly reactive for soot and then is reduced to NO itself, no band at 2133 $cm^{-1}$ is observed on the mixtures of the catalysts and soot (Fig. 10b and d).

### 3.9. $NO_x$-TPD results

As mentioned above, the differences of the FTIR results between PtAl and SPtAl (Figs. 9b and d) may come from the reason that on the PtAl sample, the $NO_x$ species mainly formed on the alumina support while on the SPtAl sample, the $NO_x$ adsorption on alumina was inhibited, providing more chances for $NO_x$-soot reactions. To further confirm this speculation, $NO_x$-TPD tests were performed.

As shown in Fig. 11, two $NO_2$ desorption peaks are observed at 60 and 310 °C on PtAl, which are associated with desorption of weakly adsorbed $NO_2$ and the decomposition of nitrates, respectively. A NO desorption peak associated with the thermodynamic-driven decomposition of $NO_2$ and/or $NO_2$ dissociation on reducible Pt sites, is observed at about 370 °C at a much lower intensity [9]. For the SPtAl sample, the $NO_2$ desorption peaks are obviously weaker and shift toward lower temperatures, indicating a reduced $NO_2$ adsorption and less stability of nitrates on this sample due to the increased acidity of the sulfated catalyst [37].

After mixed with soot, the PtAl sample desorbed $NO_2$ and NO at lower temperatures. A broad $NO_2$ peak located between 30 and 400 °C is observed for the PtAl + soot mixture, and there is significant increase in the desorption amount of NO derived from $NO_2$ decomposition. For the SPtAl + soot sample, the desorption of $NO_2$ occurs at 30–300 °C, with a sharp peak at 70 °C attributed to weakly adsorbed $NO_2$. A weak NO desorption peak at around 260 °C is also observed. The qualitative analysis of the TPD results will be given in the following discussion.

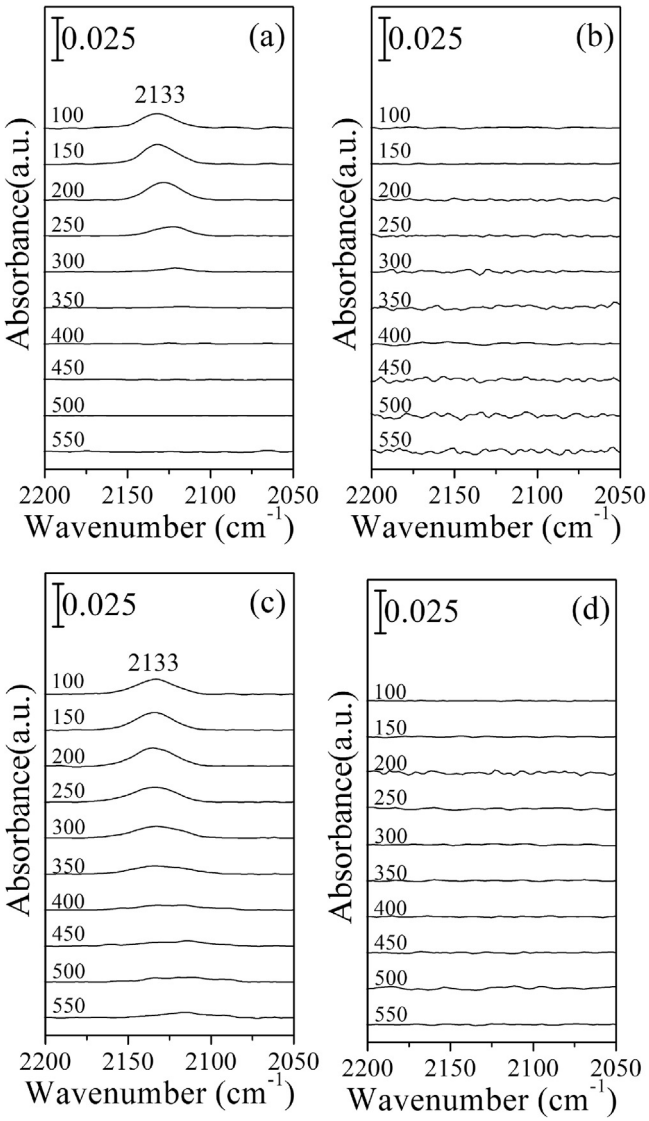


**Fig. 10.** DRIFT spectra between 2200 and 2050 $cm^{-1}$ recorded over (a) PtAl catalyst, (b) PtAl + soot mixture, (c) SPtAl catalyst, (d) SPtAl + soot mixture and (e) soot exposed to 1000 ppm $NO_2$/10% $O_2$/$N_2$ at different temperatures.

## 4. Discussion

### 4.1. Influence of sulfates on $NO_2$ utilization

In this study, with similar structure (XRD and BET results), similar Pt particle size (TEM) and lower Pt dispersion (CO titration), the sulfated catalyst SPtAl exhibits a lower soot oxidation activity in the absence of $NO_x$ than the unsulfated PtAl. On the other hand, SPtAl shows an obviously higher soot oxidation activity in the presence of $NO_x$ despite of its worse $NO_2$ production ability. It implies that gaseous $NO_x$ is indispensable for the promotion effect of sulfates on the soot oxidation activity of $Pt/Al_2O_3$ catalyst. The gaseous $NO_2$ generated at Pt active sites is necessary for the reactions since the SAl catalyst without the previous metal yields almost no activity for soot oxidation. Meanwhile, the acceleration effect of sulfates is strongly limited by the contact condition as confirmed by the soot oxidation tests in "non-contact" mode.

The importance of high efficiency of $NO \leftrightarrow NO_2 \leftrightarrow$ soot cycle has been demonstrated by some researches [37–39], which may also be one important reason for the high soot oxidation activity of the SPtAl catalyst with weakened $NO_2$ productivity. As indicated in ref. [37], the efficiency of $NO_2$ was defined by Eq. (1) as:

$$\text{Efficiency of } NO_2 = \frac{CO_2 \text{ in soot} - \text{TPO}(NO + O_2) - CO_2 \text{ in soot} - \text{TPO}(O_2)}{NO_2 \text{ in NO-TPO} - NO_2 \text{ in soot} - \text{TPO}(NO + O_2)} \quad (1)$$

In the "non-contact" mode, without the direct contact between catalysts and soot, it is unlikely for the occurrence of the $NO \leftrightarrow NO_2 \leftrightarrow$ soot cycle. In this case, the calculated $NO_2$ efficiency turns out to be 0.9 and 0.8 for PtAl and SPtAl at 375 °C (at this temperature the NO oxidation rate was maximal for both PtAl and SPtAl and the $O_2$-assisted combustion is strongly limited), respectively. This value is close to 1, indicating that hardly any NO generated in the $NO_2$-soot reaction can be reoxidized. Thus, the SPtAl catalyst exhibits a lower soot oxidation activity than PtAl in the "non-contact" mode. In the loose-contact mode, the calculated $NO_2$ efficiency is around 2.3 and 9.8 for PtAl and SPtAl, respectively. It means that SPtAl acts as a more effective catalyst for $NO_2$ utilization in the soot oxidation reaction. This may be associated with the improved oxidation-resistance of metallic platinum by interacting with the electronegative sulfates in the oxidizing atmosphere, which is important for achieving high $NO \leftrightarrow NO_2$ recycling efficiency [18,37].

On the other hand, the SPtAl catalyst may also promote the catalytic oxidation of soot via surface reactions on the sulfated support. For a soot oxidation reaction in the presence of $NO_x$, the produced $NO_2$ should be effectively transferred onto the surface of soot to initiate the creation of O-containing sites intermediates. There is a competitive adsorption of $NO_x$ on the surface of the alumina support and on the surface of soot. $\gamma$-$Al_2O_3$ is known to react with acidic molecules such as $NO_2$ because of its amphoteric nature. The acidic nature of sulfates may accelerate the transfer of the $NO_2$ formed on Pt active sites to the surface of soot instead of $NO_x$ adsorption on the alumina support, which would facilitate the reactions between $NO_x$ and soot. This speculation was verified by the $NO_x$-TPD tests. The amounts of $NO_x$ desorbed in the tests are summarized in Fig. 12. It should be always kept in mind that the NO desorbed at high temperatures in Fig. 11b derives mainly from the thermodynamic-driven

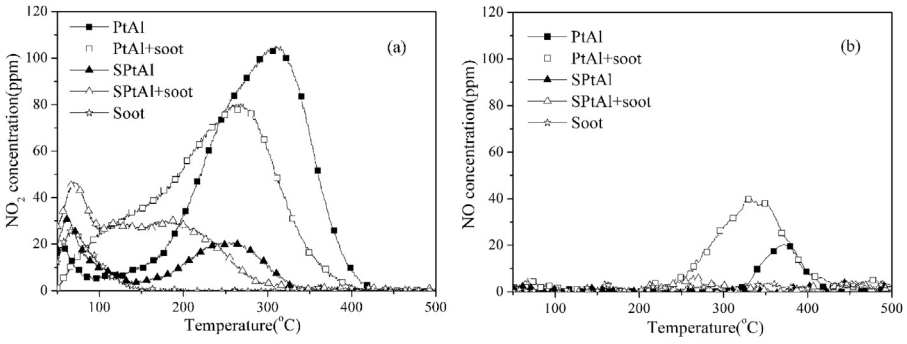


**Fig. 11.** (a) $NO_2$ and (b) NO profiles in $NO_x$-TPD of the catalysts.

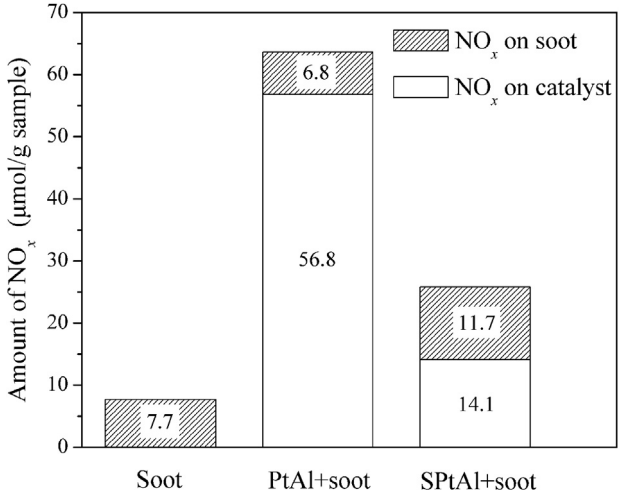


**Fig. 12.** Amounts of the $NO_x$ desorbed from different samples in the $NO_x$-TPD tests.

decomposition of $NO_2$ and/or $NO_2$ dissociation on reducible Pt sites. In this sense, the amount of $NO_x$ desorption can be considered as the amount of $NO_2$ adsorbed on the catalyst and soot. The differences between the $NO_x$ desorbed from the catalyst + soot mixtures and pure catalysts were calculated, and could be roughly taken as the $NO_x$ adsorbed on soot in the catalyst + soot mixtures.

It can be seen that the amount of $NO_x$ desorbed from soot in the PtAl + soot mixture (6.8 μmol/g sample) is even less than that from pure soot (7.7 μmol/g sample), indicating the PtAl catalyst inhibits the $NO_x$ adsorption on soot to some extent due to the strong affinity of the alumina support for nitrates. Contrarily, the sulfation of the catalyst increases the $NO_x$ desorption on the soot in despite of the greatly reduced adsorption of $NO_x$ on the pure catalyst itself. Thus, the preferential adsorption of $NO_x$ on soot with the sulfated catalyst may result in more $NO_2$-soot reactions.

Although the $NO_x$-TPD tests verified the preferential adsorption of $NO_2$ on soot promoted by the sulfates on the catalyst, the possibility that adsorption on the surface of alumina support reaches equilibrium cannot be ruled out. In this case, the preferential adsorption of $NO_2$ would not affect the $NO_2$-soot reactions. However, a similar phenomenon is observed in the DRIFT spectra obtained in the 1000 ppm $NO_2 + O_2$ atmosphere (Fig. 9), in which the $NO_2$ concentration far exceeds the maximal value (<400 ppm) that the catalysts can generate in the NO-TPO tests (Fig. 7). It implies that the adsorption equilibrium of $NO_x$ on the catalysts and soot is not easy to achieve in this study. In Fig. 9, the adsorption bands associated with nitrite species are observed at 1626, 1593, 1346, 1266 and 1204 $cm^{-1}$ on pure soot. After mixed with the PtAl catalyst, the spectra shapes are quite similar to those on PtAl without soot, only with the appearance of some extra bands corresponding to the SOCs species at high temperatures. Contrarily, the DRIFT spectra on SPtAl + soot seem likely to be a sum of the spectra on SPtAl and those on pure soot. All the soot-associated nitrates bands can be detected even in stronger intensity on the SPtAl + soot mixture, which highlights the preferential adsorption of $NO_2$ on soot. Since nitration of aromatic soot structures is one of the major steps of soot oxidation with $NO_2$, these enhanced reactions may very likely further increase the oxidation rates of soot [28].

### 4.2. Influence of sulfates on deep oxidation of SOCs

It has been reported that the $NO_2$ derived from NO oxidation would react with soot and initiate the creation of surface oxygenated complexes, SOCs, which are more reactive than the complexes that have already existed on soot. As a consequence, $O_2$ and $NO_2$ are able to react with SOCs to finally generate $CO_2$, which is also a crucial step for the catalytic oxidation of soot [9,23]. The reactions are briefly described as:

$$C_s + NO_2 \leftrightarrow C(O) + NO \quad (2)$$

$$C(O) + O_2 \rightarrow CO_2 \quad (3)$$

$$C(O) + NO_2 \rightarrow CO_2 + NO \quad (4)$$

where $C_s$ indicates the free carbon surface species and C(O) represents SOCs. The SOCs decomposition can also occur through the thermal dissociation of intermediates. However, the soot oxidation reaction was performed in the oxidizing atmosphere containing $O_2$ and/or $NO_2$. Thus, reaction 3 is suggested to dominate the decomposition of SOCs species because $O_2$ is present abundantly in comparison to $NO_2$.

It has been supposed by Oi-Uchisawa et al. that the $SO_3$ (or $H_2SO_4$) produced from $SO_2$ over Pt surfaces may accelerate the carbon oxidation, possibly by decomposing SOCs on the carbon surface, and they also emphasized the indispensable of $H_2O$ in the catalytic reactions [40]. However, their speculations are lacking in proof of experiments. In this study, it is observed by the TGA and *ex situ* FTIR that the addition of sulfates on the $Pt/Al_2O_3$ catalyst results in a similar promotion effect with the dehydration of catalyst, i.e. the participation of surface hydroxyl on the alumina support. As shown in the in situ FTIR spectra obtained in the reaction atmosphere (Fig. 8), distinct bands assigned to carbon oxygen functionalities such as anhydride, lactones and/or carboxylic species are observed on the unsulfated sample mixed with soot, which cannot be detected on the SPtAl + soot mixture. This implies that the sulfate species either inhibit the formation of SOCs, or accelerate their decomposition. Furthermore, the sulfation of $Pt/Al_2O_3$ catalyst leads to a preferential adsorption of $NO_x$ on the surface of soot and may accelerate the formation of SOCs. Then, it is more likely that the sulfated catalyst accelerate the decomposition of partially oxidized carbon species.

The promotion effect of sulfate species on the decomposition of SOCs is confirmed by the catalytic oxidation tests of the $NO_2$-pretreated soot (Nsoot). Nsoot represents the soot that is firstly attacked by $NO_2$ and surface oxygen complexes are produced (Reaction (1)). As shown in Tables 3 and 4, the pretreatment in $NO_2$ even inhibits the catalytic oxidation of Nsoot over PtAl to some extent since the most readily oxidizable surface species have been consumed in the pretreatment. On the contrary, the catalytic oxidation of Nsoot over SPtAl is accelerated significantly, and a similar promotion effect is observed over SAl. These indicate that the sulfate species may accelerate the decomposition of the partially oxidized surface species even without precious metals. It has been reported by Mehring that, in the presence of $NO_2$, $H_2SO_4$ may increase the amount of $NO_2^+$ on soot, which is the known active species for the nitration of aromatic structures [28]. They suggested that the nitrified aromatic system is more easily to be further oxidized, leading to ring-opening and decomposition of the aromatic system by decarboxylation and decarbonylation. This speculation is confirmed by the in situ FTIR results obtained in $NO_2$ and $O_2$ (Fig. 10), which demonstrate the high reactivity of $NO_2^+$ with soot and the effect of sulfates on the stability of $NO_2^+$.

On the basis of in situ characterization results and the above discussion, the reaction mechanism for soot oxidation on surface of the sulfated $Pt/Al_2O_3$ catalyst in the presence of $NO_x$ can be proposed. There are two main promotion effects of the sulfate species over the surface reactions during soot oxidation: (1) the acidic nature of sulfates inhibits the adsorption of $NO_x$ on the alumina support, leading to a preferential adsorption of $NO_x$ on the surface of soot and hereby

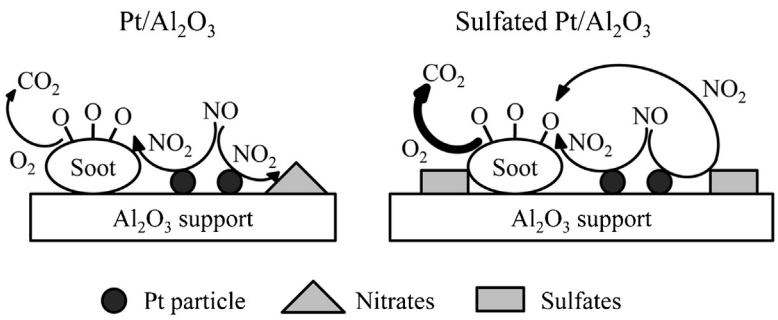


**Fig. 13.** Mechanism illustration of soot oxidation over $Pt/Al_2O_3$ and sulfated $Pt/Al_2O_3$ in the presence of $NO + O_2$.

more chances for $NO_x$-soot reactions; (2) the sulfate species accelerate the decomposition of surface oxygen complexes that form on the surface of soot attacked by $NO_2$, followed by the soot being fully oxidized. The scheme of this surface reaction process is described in Fig. 13.

## 5. Conclusions

Sulfation of $Pt/Al_2O_3$ catalyst leads to a slightly destruction of the catalyst structure, resulting in decreases in the BET surface area and the amount of Pt active sites. The TOF values of SPtAl and PtAl catalysts for NO oxidation and soot oxidation in $O_2$ are similar to each other since they have similar Pt particle size distribution. With a reduced exposed Pt surface area by the coverage of sulfates, the sulfated catalyst exhibits worsened catalytic activities for NO oxidation and soot oxidation in $O_2$. However, the sulfated $Pt/Al_2O_3$ shows much higher activities for the oxidation of soot in the presence of $NO_x$. The TOF values obtained at 300 °C are $5.79 \times 10^{-3}$ and $3.73 \times 10^{-3}\ s^{-1}$ for SPtAl and PtAl catalysts, respectively.

This "abnormal" high $NO_x$-assisted soot oxidation activity of the sulfated catalysts can be explained by the synergistic effects of the sulfate species and platinum/alumina. In the soot oxidation reactions, the role of platinum is to oxidize NO to $NO_2$ which attacks soot to produce surface oxygenated complexes. In spite of the reduced NO oxidation activity of the sulfate catalyst, the electronegative sulfate species may improve the oxidation-resistance of metallic platinum in the oxidizing atmosphere, which is important for achieving high $NO \leftrightarrow NO_2 \leftrightarrow$ soot recycling efficiency. Meanwhile, the amount of $NO_x$ desorbed from soot in the SPtAl + soot mixture (11.7 μmol/g sample) is about two times of that in the PtAl + soot mixture (6.8 μmol/g sample) according to the $NO_x$-PD results. It indicates that the acidic sulfate species inhibit the $NO_x$ adsorption on the alumina support and promote the preferential adsorption of $NO_x$ on soot, providing more chances for $NO_2$-oot reactions.

More importantly, the further decomposition of SOCs can be accelerated by sulfates, which is confirmed by the catalytic oxidation tests of the $NO_2$-retreated soot in $O_2$. The TOF values are $3.63 \times 10^{-3}$ and $0.93 \times 10^{-3}\ s^{-1}$ for SPtAl and PtAl catalysts, respectively. Such a promotion effect of sulfates exists even on the SAl catalyst without precious metal. Thus, high catalytic efficiency for soot oxidation is achieved on the sulfated $Pt/Al_2O_3$ catalyst.

## Acknowledgements

The authors would like to acknowledge Projects 2013AA061902 and 2010CB732304 by the Ministry of Science and Technology of China.

## Appendix A. Supplementary data

Supplementary data associated with this article can be found, in the online version, at http://dx.doi.org/10.1016/j.apcatb.2013.02.053.

## References

[1] P.A. Kumar, M.D. Tanwar, S. Bensaid, N. Russo, D. Fino, Chemical Engineering Journal 207–208 (2012) 258–266.
[2] S.S. Gross, M.A. Ulla, C.A. Querini, Journal of Molecular Catalysis A 352 (2012) 86–94.
[3] J. Oi-Uchisawa, A. Obuchi, R. Enomoto, S.T. Liu, T. Nanba, S. Kushiyama, Applied Catalysis B 26 (2000) 17–24.
[4] J. Oi-Uchisawa, A. Obuchi, R. Enomoto, J.Y. Xu, T. Nanba, S.T. Liu, S. Kushiyama, Applied Catalysis B 32 (2001) 257–268.
[5] J.P.A. Neeft, O.P. van Pruissen, M. Makkee, J.A. Moulijn, Applied Catalysis B 12 (1997) 21–31.
[6] J. Liu, Z. Zhao, J.Q. Wang, C.M. Xu, A.J. Duan, G.Y. Jiang, Q. Yang, Applied Catalysis B 84 (2008) 185–195.
[7] Y.C. Wei, J. Liu, Z. Zhao, A.J. Duan, G.Y. Jiang, Journal of Catalysis 287 (2012) 13–29.
[8] J.H. Pazmiño, J.T. Miller, S.S. Mulla, W.N. Delgass, F.H. Ribeiro, Journal of Catalysis 282 (2011) 13–24.
[9] X.D. Wu, F. Lin, H.B. Xu, D. Weng, Applied Catalysis B 96 (2010) 101–109.
[10] X.D. Wu, S. Liu, F. Lin, D. Weng, Journal of Hazardous Materials 181 (2010) 722–728.
[11] N. Guillén-Hurtado, A. Bueno-López, A. García-García, Applied Catalysis A 437–438 (2012) 166–172.
[12] I. Atribak, F.E. López-Suárez, A. Bueno-López, A. García-García, Catalysis Today 176 (2011) 404–408.
[13] S. Liu, X.D. Wu, D. Weng, M. Li, H.R. Lee, Chemical Engineering Journal 203 (2012) 25–35.
[14] L.S. Escandón, Salvador Ordóñez, A. Vega, F.V. Díez, Journal of Hazardous Materials 153 (2008) 742–750.
[15] A. Boubnov, S. Dahl, E. Johnson, A.P. Molina, S.B. Simonsen, F.M. Cano, S. Helveg, L.J. Lemus-Yegres, J.D. Grunwaldt, Applied Catalysis B 126 (2012) 315–325.
[16] K. Villani, W. Vermandel, K. Smets, D.D. Liang, G.V. Tendeloo, J.A. Martens, Environmental Science and Technology 40 (2006) 2727–2733.
[17] K. Chakarova, M. Mihaylov, K. Hadjiivanov, Microporous and Mesoporous Materials 81 (2005) 305–312.
[18] Y. Yazawa, N. Takagi, H. Yoshida, S. Komai, A. Satsuma, T. Tanaka, S. Yoshida, T. Hattori, Applied Catalysis A 233 (2002) 103–112.
[19] H. Wijnja, C.P. Schulthess, Spectrochimica Acta, Part A 55 (1999) 861–872.
[20] R.L. Frost, J. Kloprogge, S.C. Russell, J.L. Szetu, Thermochimica Acta 329 (1999) 47–56.
[21] M. Skoglundh, A. Ljungqvist, M. Petersson, E. Fridell, Applied Catalysis B 30 (2001) 315–328.
[22] M.L. Guzmán-Castillo, E. López-Salinas, J.J. Fripiat, J. Sánchez-Valente, F. Hernández-Beltrán, A. Rodríguez-Hernández, J. Navarrete-Bolaños, Journal of Catalysis 220 (2003) 317–325.
[23] A. Setiabudi, M. Makkee, J.A. Moulijn, Applied Catalysis B 50 (2004) 185–194.
[24] B. Azambre, S. Collura, J.M. Trichard, J.V. Weber, Applied Surface Science 253 (2006) 2296–2303.
[25] H. Muckenhuber, H. Grothe, Carbon 44 (2006) 546–559.
[26] J. Zawadzki, M. Wiśniewski, K. Skowrońska, Carbon 41 (2003) 235–246.
[27] P. Ciambelli, V. Palma, P. Russo, S. Vaccaro, Catalysis Today 60 (2000) 43–49.
[28] M. Mehring, M. Elsener, L. Bächli, O. Kröcher, Carbon 50 (2012) 2100–2109.
[29] R. Marques, P. Darcy, P.D. Costa, H. Mellottée, J-M. Trichard, G. Djéga-Mariadassou, Journal of Molecular Catalysis A 221 (2004) 127–136.
[30] M. Kantcheva, E.Z. Ciftlikli, Journal of Physical Chemistry B 106 (2002) 3941–3949.
[31] I.S. Pieta, M. García-Diéguez, C. Herrera, M.A. Larrubia, L.J. Alemany, Journal of Catalysis 270 (2010) 256–267.

[32] Y. Su, M.D. Amiridis, Catalysis Today 96 (2004) 31–41.
[33] K.I. Hadjiivanov, Catalysis Reviews 42 (2000) 71–144.
[34] T.J. Toops, D.B. Smith, W.P. Partridge, Applied Catalysis B 58 (2005) 245–254.
[35] H. Muckenhuber, H. Grothe, Carbon 45 (2007) 321–329.
[36] J.L. Flores-Moreno, G. Delahay, F. Figueras, B. Coq, Journal of Catalysis 236 (2005) 292–303.
[37] X.D. Wu, S. Liu, D. Weng, Catalysis Science & Technology 1 (2011) 644–651.
[38] A. Setiabudi, M. Makkee, J.A. Moulijn, Applied Catalysis B 42 (2003) 35–45.
[39] A. Setiabudi, B.A.L. van Setten, M. Makkee, J.A. Moulijn, Applied Catalysis B 35 (2002) 159–166.
[40] J. Oi-Uchisawa, A. Obuchi, A. Ogata, R. Enomoto, S. Kushiyama, Applied Catalysis B 21 (1999) 9–17.